PERGAMON

International Journal of Multiphase Flow 24 (1998) 721–737

International Journal of Multiphase Flow

Two-fluid model studies for high density two-phase liquid metal vertical flows

P. Satyamurthy [a], N.S. Dixit [a], T.K. Thiyagarajan [a], N. Venkatramani [a], A.M. Quraishi [b], A. Mushtaq [b]

[a] *Laser and Plasma Technology Division, Bhabha Atomic Research Centre, Mumbai-400085, India*
[b] *Department of Physics, Aligarh Muslim University, Aligarh-202002, India*

Received 18 May 1997; received in revised form 2 November 1997

Abstract

Liquid metal magnetohydrodynamic power converters (LMMHD PC) have been recently proposed for electrical power generation. These systems contain two-phase vertical flows consisting of high density liquid metals and suitable gas–vapor. Optimum design of LMMHD power plants require accurate modeling of two-phase flows in the riser. A two-fluid model has been developed for this purpose. One-dimensional, steady state two-fluid flow equations consisting of conservation of mass, momentum of each phase along with auxiliary relations have been solved numerically by the Runge–Kutta method. Interfacial drag force corresponding to multi-bubble, churn turbulent and slug flow based on Ishii et al. and Taitel classification has been used. Effect of variation of void fraction and phase velocities of the fluids across the cross section of the pipe has been studied based on Ishii et al. model by modifying relative velocity and incorporating appropriate coefficients in the conservation equations. Bubble size at the mixer orifice exit has been calculated using the equations of Kumar et al. In order to verify the accuracy of the model, a nitrogen–mercury experimental system has been set up. Void profiles have been measured using gamma-ray attenuation method. Void fraction, slip and pressure at different locations were determined for the mass fluxes varying from 0.125 to 2.302 kg/sm^2 for nitrogen and 5.52×10^3 to 12.26×10^3 kg/sm^2 for mercury. The predicted values have been compared with the experimental data. The void fraction values matched well with the experimental data within 10% and within 20% when cross-sectional effects were included. The over all pressure values were within 13% and 8%, respectively, while the slip values deviated within 25% and 27%, respectively. In general, the model matched better with experimental data when the cross-sectional effects were not included. This is due to the high density of the liquid metal and relatively larger pipe diameter.

Keywords: Bubble distribution; Churn turbulent; Electrodynamic fluid; Gravity type; Jet flow; Liquid metal MHD; Mercury–nitrogen; Mixer; Multi-bubble; Power conversion; Separator; Slug; Thermodynamic fluid; Two-fluid flow; Two-phase; Void fraction

0301-9322/98/$19.00
PII: S0301-9322(97)00086-4

1. Introduction

Liquid metal magneto hydrodynamic power converters (LMMHD PC) of gravity type have been recently proposed for electrical power generation as an alternate to turbine route for various heat sources, i.e. fossil, solar, nuclear and industrial waste etc. (Branover, 1993; Barak et al., 1990; Satyamurthy et al., 1995). In these systems, two-phase flows consisting of steam and high density liquid metal (lead, lead–bismuth alloy etc.) take place in the riser pipe and liquid metal flow in the downcomer pipe containing MHD generator. The LMMHD PC have large conversion efficiency in view of isothermal expansion in the riser pipe (as against adiabatic expansion of steam in turbine of Rankine cycle). A cogeneration LMMHD system based on fossil fuel is at an advanced stage of commercialization.

However, to design a large size power system as well as improve the conversion efficiency, basic studies, both experimental and theoretical are required to be carried out in these systems. The areas of interest are two-phase flows in the riser pipe with the void fraction varying from $\leqslant 0.1$ near the mixer exit to $\backsim 0.8$ at the separator entrance. It is in the riser pipe that the mechanical work done by the vapor (isothermal expansion) is transferred to the liquid metal and decides the over all energy conversion. The pressure head, created due to density difference (which is a strong function of void fraction), is balanced against the pressure head due to MHD force, frictional pressure drop etc. The void distribution in the riser is decided by the interfacial drag force, virtual mass force etc. Accurate prediction of void fraction distribution in the riser is essential for designing the LMMHD PC systems.

Various two-phase models based on air–water, steam–water and, to a limited extent, liquid metal are available. Most of the studies in two phase liquid metal flows have been confined to diffusion model, where the two-phases are considered as a single fluid with empirical relation for void fraction (Serizawa and Michiyoshi, 1973; Dounan et al., 1985; Unger et al., 1986; El-Boher et al., 1988). Even though the diffusion model is simple, compared to the two-fluid model, many important characteristics of two-phase flow are lost (e.g. initial conditions of the mixer can not be incorporated in the flow, void fraction can not be determined explicitly from the equations etc.). For liquid metal two-phase flows, studies have been carried out with multi-bubble two-fluid model (Mond and Sukoriansky, 1984; Eckert et al. 1993). However, the actual flow evolves from multi-bubble to churn-turbulent to slug flow along the riser.

In this paper, a two-fluid model is developed based on the work of Ishii and others (Ishii and Zuber, 1979; Ishii and Mishima, 1984) and has been used for nitrogen–mercury two-phase upward vertical flows. The predicted void fraction, slip and pressure are compared with the experimental values. The applicability of this model for high density liquid metal two-phase flows has also been discussed. In view of this an LMMHD experimental facility consisting of nitrogen–mercury was set up.

2. Experimental facility

Nitrogen and mercury were chosen in view of their similar properties with lead/lead alloys and steam which have been proposed for commercial LMMHD PC as shown in Table 1.

Table 1
Properties of thermodynamic and electrodynamic fluids

Parameters	Electrodynamic fluids		
	Mercury	Lead	lead-bismuth
	30°C	∽400°C	∽200°C
Density (kg/m^3)	1.355×10^4	1.050×10^4	1.05×10^4
Electrical Conductivity (S/m)	1.016×10^6	1.020×10^6	1.058×10^6
Surface Tension (N/m)	0.472	0.462	0.402
Viscosity (kg/ms)	0.155×10^{-2}	0.2141×10^{-2}	0.2137×10^{-2}
	Thermodynamic fluids		
	Nitrogen	Steam	
	∽30°C	∽400°C	
Viscosity (kg/ms)	1.67×10^{-5}	2.48×10^{-5}	

Schematic of the experimental facility is shown in Fig. 1. The system consists of mixer, riser pipe, separator, downcomer pipe, MHD generator, diffuser etc.

The mixer was made of stainless steel of 0.35 m length and internal diameter of 0.168 m and included 0.15 m of nozzle connecting the riser pipe as shown in Fig. 2. It also consisted of a pair of horizontal pipes of 20 mm NB, having in each 30 holes of 1.4 mm diameter distributed equally along the distributor length confined to the top half. The number of holes were decided such that the pressure drop in the distributor was less than 0.005 bar.

Both riser and downcomer pipes were made up of stainless steel of internal diameter 79.0 mm. Pressure transmitters were installed at four locations along the riser pipe (0.64, 1.93, 2.69 and 3.48 m). In the riser at locations 1.1. and 2.8 m above the mixer, a gamma ray source along with the detector system was installed for measuring void fraction profiles using the gamma ray attenuation method (Thiyagarajan et al., 1995). The schematic of the measurement system is shown in Fig. 3. ^{60}Co of activity 2775 MBq was used as gamma ray source and 1.33 MeV photons were chosen for measurements. Radioactive source was placed in a lead container and a 3 mm diameter beam was obtained. The detector unit consisting of NaI(Tl) scintillator, photo multiplier tube and pre-amplifier, was connected to a gamma ray spectrometer. The source and the detector were mounted on a horizontally movable platform so that the gamma ray beam could pass through various chord lengths of the cross-section of the pipe. The pulse height analyzer was set so that only 1.33 MeV energy gamma rays were counted. The measurements were taken at various chord lengths corresponding to the counts when the pipe was filled with nitrogen only, mercury only and during the two-phase flow.

Nitrogen was introduced into the mixer from the header at 6–7 kg/cm^2 pressure and was separated and let out to the ambient. Mercury alone flowed through the downcomer and the MHD generator.

2.1. Method of void fraction determination

Because of extreme complexity of two-phase flows, most of the well known empirical relations and models give area averaged void fractions. Since void fraction varies across the

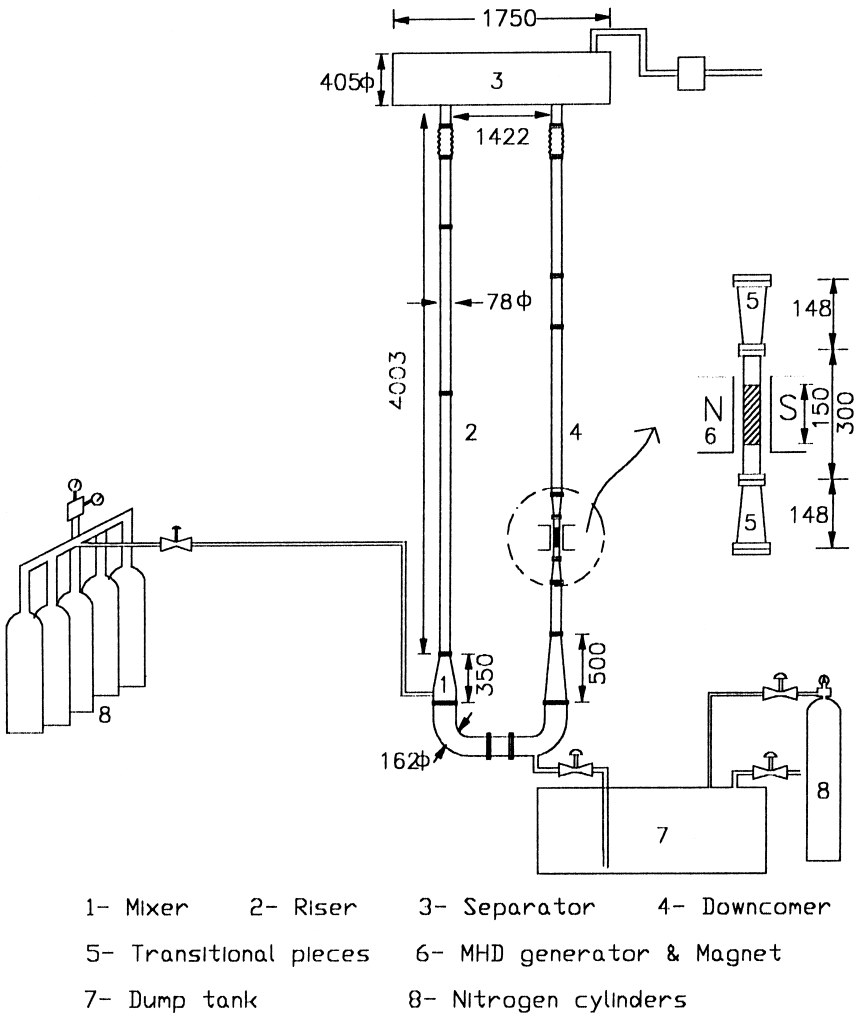

Fig. 1. Schematic of the nitrogen–mercury LMMHD experimental facility.

cross-section of the pipe, to determine averaged void fraction, void fraction profiles as a function of radial distance should be determined. This was determined as follows.

The cross-section of the two-phase flow in the pipe was assumed to have a number of circular zones having uniform void fraction in each zone as shown in the Fig. 4. Assuming 'm' circular zones of void fractions α_1, α_2, α_3, ..., α_j, ..., α_m which were to be determined, let β_1, β_2, β_3 ..., β_i, ..., β_n be the measured void fractions at the various chord lengths. Then we have:

$$\beta_i = \sum_{j=1}^{m} \frac{d_{ij}}{c_i} \alpha_j. \tag{1}$$

where c_i was the total path length for the gamma ray at the ith chord length and d_{ij} was the

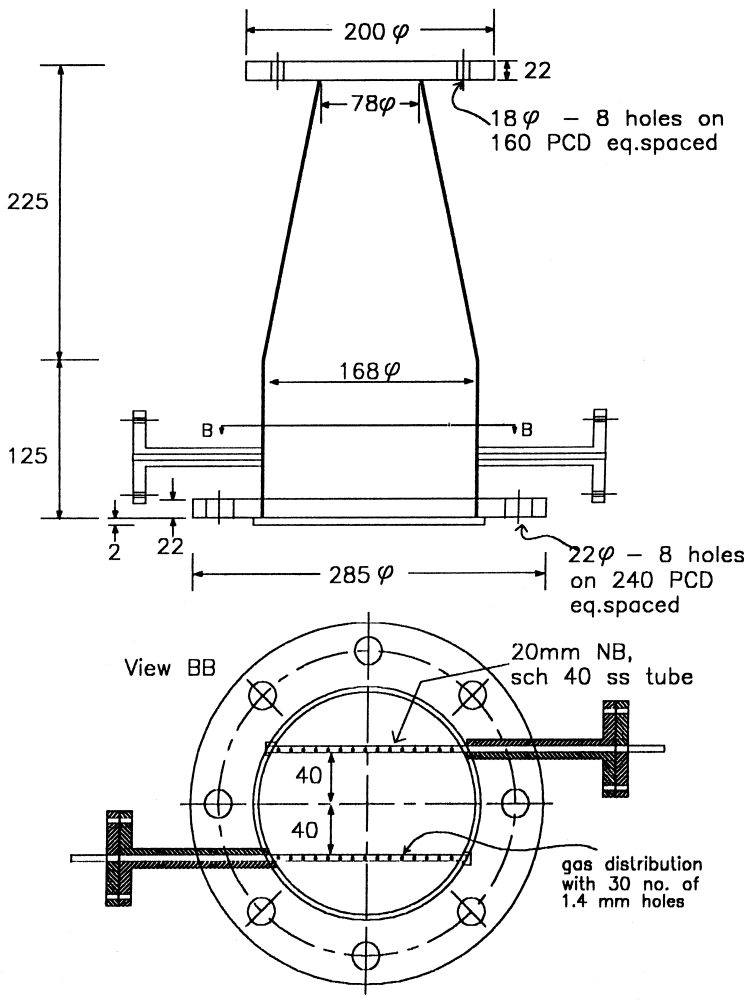

Fig. 2. Details of the mixer.

length of the jth zone intercepted by the gamma ray bean at the ith chord length. β_is were obtained from measured gamma ray intensities at the ith chord with gas alone ($I_{i,g}$), with liquid metal alone ($I_{i,l}$) and when two-phase flow was present ($I_{i,t}$) and are given by

$$\beta_i = \frac{\ln(I_{i,t}/I_{i,l})}{\ln(I_{i,g}/I_{i,l})}. \tag{2}$$

Let E be the error function defined as follows

$$E^2 = \left(\sum_{i=1}^{n} \beta_i - \sum_{j=1}^{m} \frac{d_{ij}}{c_i} \alpha_j \right)^2. \tag{3}$$

The minimization of E with respect to the m parameters of $\alpha_1, \alpha_2, \alpha_3, \ldots, \alpha_j, \ldots, \alpha_m$ gives a set

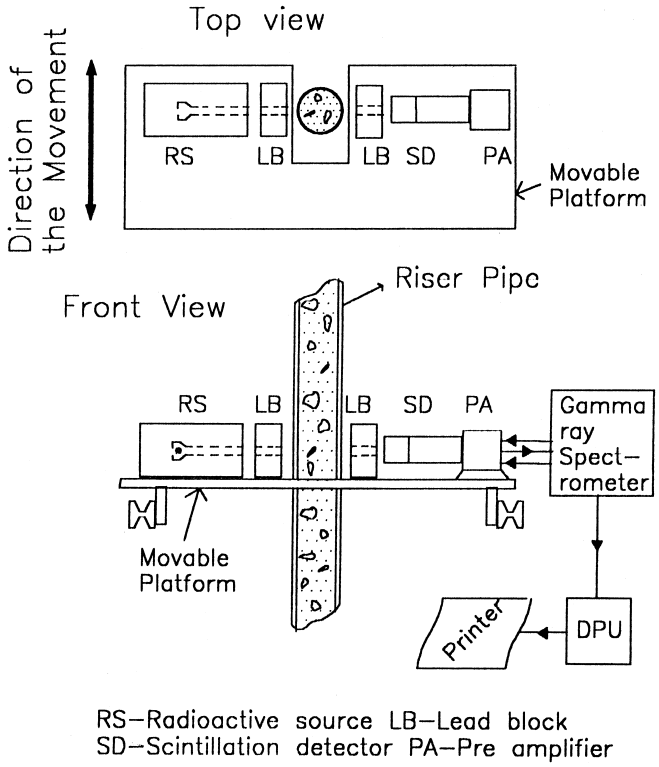

Fig. 3. Schematic of the void fraction measurement system.

of 'm' linear equations. Using the measured values of β_1, β_2, β_3, ..., β_i, ..., β_n, the values of α were obtained. In a typical experiment, the number of chords chosen was 38 with 2.0 mm spacing and seven zones were assumed. From the void fraction profiles, the area averaged void fraction was determined. The beam diameter (3 mm) was chosen so that finite beam errors were negligible (Satyamurthy et al., 1994) besides obtaining a large number of zones. Number of counts were taken in excess of 6000 for every measurement so that statistical fluctuations were negligible ($<1.5\%$) (Munshi and Vaidya, 1993). In addition, dynamic void fluctuation corrections were estimated to determine the error range in the analysis (Thiyagarajan et al., 1991).

3. Flow modeling

3.1. Gas flow through the orifice of the mixer

The type of the bubble generated in the mixer is very crucial for the overall power conversion. Ideally, the larger number of bubbles for a given flow rate, the better it is. This increases drag force, thus reducing the slip and increasing the void fraction. As described

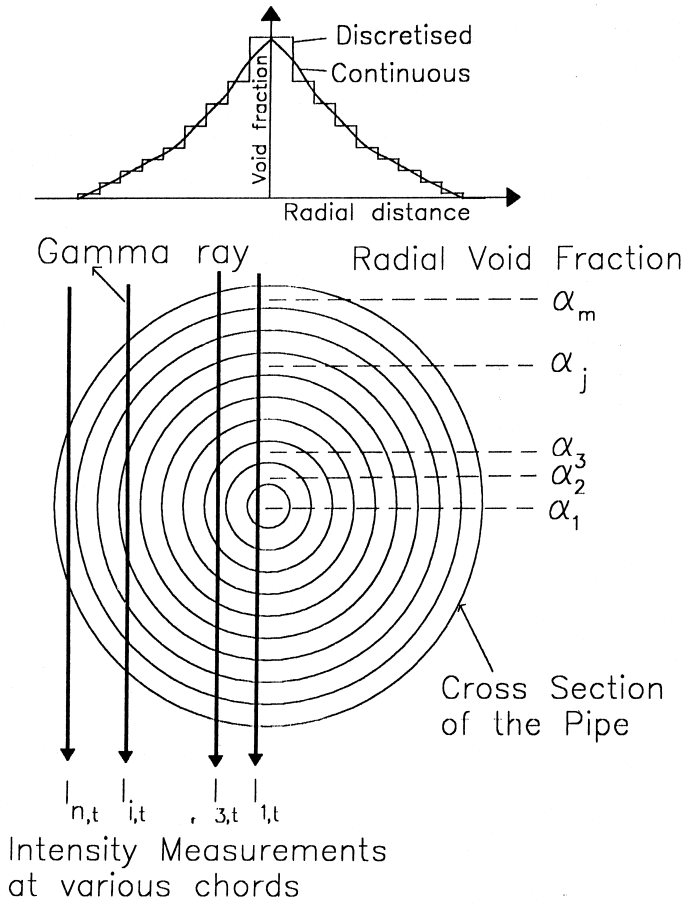

Fig. 4. Scheme for the measurement of void fraction profile.

earlier, the mixer distributor used in our facility consisted of 60 holes of 1.4 mm diameter. The nitrogen gas at the exit of the orifice of the distributor could come out either as a bubble or as a turbulent jet depending upon the flow rate. The jet consists of large, closely spaced irregular bubbles with swirling motion. These bubbles disintegrate into smaller ones of random distribution. No detailed studies have been carried out for liquid metal–gas flows to study bubble size distribution. In view of this, bubble diameters for various gas flows have been determined by using Kumar et al. (1976) relations as given below. These relations are based on the experiments carried out with air–water/kerosene/glycerol.

Table 2
Effective bubble diameter for various gas flow-rates

$\dot{m}_g \times 10^3$ [kg/s]	D_b [mm]
0.6	7.8
1.3	10.2
2.5	7.4
4.7	5.7
7.0	4.8
9.0	4.4
11.0	4.0

$$D_b = 1.56(N_{Re}^{0.058})\left\{\frac{\Sigma_l D_h^2}{(\rho_l - \rho_g)g}\right\}^{1/4} \quad \text{for } 1 < N_{Re} < 10 \tag{4a}$$

$$D_b = 0.32(N_{Re}^{0.425})\left\{\frac{\Sigma_l D_h^2}{(\rho_l - \rho_g)g}\right\}^{1/4} \quad \text{for } 10 < N_{Re} < 2100 \tag{4b}$$

$$D_b = 100(N_{Re}^{-0.4})\left\{\frac{\Sigma_l D_h^2}{(\rho_l - \rho_g)g}\right\}^{1/4} \quad \text{for } 4000 < N_{Re} < 70\ 000, \tag{4c}$$

where D_b is the bubble diameter, Σ_l is the surface tension of the liquid, g is the acceleration due to gravity, D_h is the orifice diameter, N_{Re} is the gas Reynolds number based on orifice diameter. Eq. (4a) and (4b) predict increasing bubble diameter, while Eq. (4c) predicts monotonically decreasing bubble diameter with N_{Re}. Since no equation is available for N_{Re} between 2100 and 4000, appropriate interpolation has to be carried out. Based on the above equations, the D_b for various flow rates were determined as shown in Table 2. These values were taken as initial bubble diameters for solving bubble momentum equation in the riser pipe. Pressure drop for the nitrogen flow in the orifice of the mixer was determined by assuming deep orifice approximation (Idelchik, 1980). The calculated pressure drop for the highest flow rate was around 0.005 bar.

3.2. Two-fluid flow model

A quasi one-dimensional steady state two fluid model, which explicitly takes into consideration gas momentum equation, has been developed. The following conservation and other auxiliary equations have been used.

Liquid metal and gas continuity equations:

$$\rho_l u_l (1 - \alpha) A = \dot{m}_l \tag{5}$$

$$\rho_g u_g \alpha A = \dot{m}_g, \tag{6}$$

where ρ, u, $\dot{m}$ are the density, velocity and mass flow rates, respectively. Subscripts l and g

correspond to liquid metal and gas, α is the area averaged void fraction and A is the internal cross-section area of the pipe.

Combined two-phase momentum equation:

$$\alpha\rho_g u_g \frac{du_g}{dz} + (1-\alpha)\rho_l u_l \frac{du_l}{dz} = -\frac{dP}{dz} - \{\alpha\rho_g + (1-\alpha)\rho_l\}g - \Phi_{lo}^2\left(\frac{dP}{dz}\right)\text{frlo}, \tag{7}$$

where z is the distance from the mixer exit, g is the acceleration due to gravity and P is the pressure. The last term is due to wall friction. It is determined by assuming the entire flow as that of liquid metal only and multiplying by the square of Φ_{lo} (two-phase multiplier) and is determined based on Friedel correlation (1979) as follows:

$$\Phi_{lo}^2 = (1-X)^2 + X^2\frac{\rho_l f_{go}}{\rho_g f_{lo}} + \left(3.24(X^{0.78}(1-X)^{0.24})\left(\frac{\rho_l}{\rho_g}\right)^{0.91}\left(\frac{\mu_g}{\mu_l}\right)^{0.19}\left(1-\frac{\mu_g}{\mu_l}\right)^{0.7}\Big/ F_r^{0.045} W_e^{0.035}\right) \tag{8}$$

where

$$F_r = \frac{G^2}{gD\rho_t^2}, \quad W_e = \frac{G^2 D}{\rho_t \Sigma_l}, \quad \rho_t = \frac{\rho_l\rho_g}{X\rho_l + (1-X)\rho_g} \quad \text{and} \quad G = \frac{(\dot{m}_l + \dot{m}_g)}{A},$$

where X is the quality and D is the internal diameter of the pipe. μ is the viscosity, Σ is the surface tension and f_{lo}, f_{go} are the friction factors with liquid and gas properties, respectively. f_{lo} is determined based on Colebrook equation (Giles, 1983) as follows:

$$\frac{1}{\sqrt{f_{lo}}} = -2\log\left(\frac{\varepsilon}{3.7D} + \frac{2.51}{N'_{Re}\sqrt{f_{lo}}}\right), \tag{9}$$

where ε is the internal surface roughness factor of the pipe and N'_{Re} is the Reynolds number of flow in the pipe. Similar equation is used for the gas. The frictional pressure drop assuming the flow to have liquid metal properties has been determined as follows:

$$\left(\frac{dP}{dz}\right)_{\text{frlo}} = \frac{8f_{lo}\dot{m}_l + \dot{m}_g)^2}{D^5\pi^2\rho_l}.$$

Momentum equation of the gas:

$$\rho_g u_g \frac{du_g}{dz} = -\frac{dP}{dz} - \rho_g g - \frac{F_D}{V_b} - \frac{F_{VM}}{V_b}, \tag{10}$$

where V_b is the effective bubble volume, and F_D and F_{VM} are the interfacial drag force and virtual mass force, respectively. Wall shear stress term in the gas momentum equation has been neglected due to low void fraction near the wall (Thiyagarajan et al., 1995). Also the interfacial shear stress, which is a function of void fraction gradient is important only in annular flows and, hence, is not included (Ishii and Mishima, 1984).

Equation of state of the gas:

$$P = \rho_g RT, \tag{11}$$

where R is the gas constant and the temperature of gas/liquid, T, is assumed to be constant. Classification of the flow structure is determined based on Taitel et al. (1980) as follows. For void fraction (α) less than 0.25, the flow is assumed to be in the multi-bubble regime. Beyond that, the flow is churn-turbulent or slug depending upon whether z is less than the entrance length 'l_E' or not. The interfacial drag force is determined based on Ishii and Mishima work.

For the multi-bubble regime, the drag force is determined as follows:

$$F_D = 0.5\rho_l V_b \sqrt{\frac{g(\rho_l - \rho_g)}{\Sigma_l}} \left\{ \frac{1 + 17.67(1-\alpha)^{9/7}}{18.67(1-\alpha)^{1.5}} \right\}^2 (u_g - u_l) \mid u_g - u_l \mid . \tag{12a}$$

When α is greater than 0.25 and z is less than entrance length l_E, then flow is churn turbulent and the drag force is given by

$$F_D = (4/3)\rho_l A_d (1-\alpha)^2 (u_g - u_l) \mid u_g - u_l \mid, \tag{12b}$$

where A_d is the projected area of the bubble. The entrance length l_E is defined as:

$$\frac{l_E}{D} = 40.6\left[\frac{\alpha u_g + (1-\alpha)u_l}{\sqrt{gD}} + 0.22\right],$$

and for the slug flow, the drag force is given by

$$F_D = 4.9\rho_l A_d (1-\alpha)^3 (u_g - u_l) \mid u_g - u_l \mid . \tag{12c}$$

The virtual mass force (F_{VM}) is determined from the following equation developed for multi-bubble flow by Zuber (1964). For all regimes of the flow, F_{VM} was found to be two or more orders less than the drag force and hence the flow was insensitive to it (Lahey et al., 1980). In view of this, the same relation is used for all the regimes.

$$F_{VM} = 0.5\frac{(1+2\alpha)}{(1-\alpha)} V_b \rho_l u_g \frac{d}{dz}(u_g - u_l). \tag{13}$$

3.3. Effect of cross-sectional variation

Ishii and Mishima have proposed that under the following conditions, the pipe diameter should be considered small.

$$\alpha < \frac{1}{C_0} \quad \text{and} \quad j_g \sqrt{\frac{\rho_g}{(\rho_l - \rho_g)gD}} > \alpha - 0.1,$$

where j_g is gas volumetric flux and C_0 is given by

Table 3
Flow rates and mass fluxes of nitrogen and mercury

$\dot{m}_g \times 10^3$ [kg/s]	G_g [kg/sm^2]	$\dot{m}_l$ [kg/s]	$G_l \times 10^{-3}$ [kg/sm^2]
0.6	0.13	26.4	5.52
1.3	0.27	28.9	6.05
2.5	0.52	35.3	7.39
4.7	0.98	43.0	9.0
7.0	1.47	48.0	10.05
9.0	1.88	54.8	11.47
11.0	2.30	58.6	12.26

$$C_0 = 1.2 - 0.2\sqrt{\frac{\rho_g}{\rho_l}}.$$

When the above conditions are satisfied, the cross-sectional variation of α and phase velocities should be taken into consideration by modifying the relative velocities of the phases as follows:

$$(u_g - u_l) \Rightarrow \frac{1 - C_0\alpha}{1 - \alpha}(u_g - C_0 u_l). \tag{14}$$

The flow and geometry of our experimental system did not satisfy the above equations except at very low gas flow rate and near the mixer entrance. This is primarily due to the large density of mercury. However, analysis has been done for both with and without cross-sectional variation effects and compared with the experimental values. The above equations were simplified algebraically and the modified non-linear equations were solved by 4th order Runge–Kutta method.

4. Experiment and analysis

Two-phase flow parameter have been calculated with the measured gas and liquid metal flow rates and mixer pressure as inputs. Experiments were carried out for various flow rates and corresponding mass fluxes as summarized in Table 3. Mercury flow rate was measured from open circuit voltage of the MHD generator and that of nitrogen by rotameter and pressure gauge near the mixer entrance. Mixer entrance pressure is determined by subtracting appropriate pressure drop in the entrance pipe line and in the orifice. Two phase parameters in the riser have been calculated based on measured flow rates of mercury and nitrogen using the above equations.

4.1. Two-phase flow in the riser

For low nitrogen flow rates and the corresponding mercury flow rates, the void exhibits oscillating profile as a function of radial coordinate at both locations as shown in Fig. 5. Also there is a significant asymmetry between the left and the right profiles. In view of this, spread

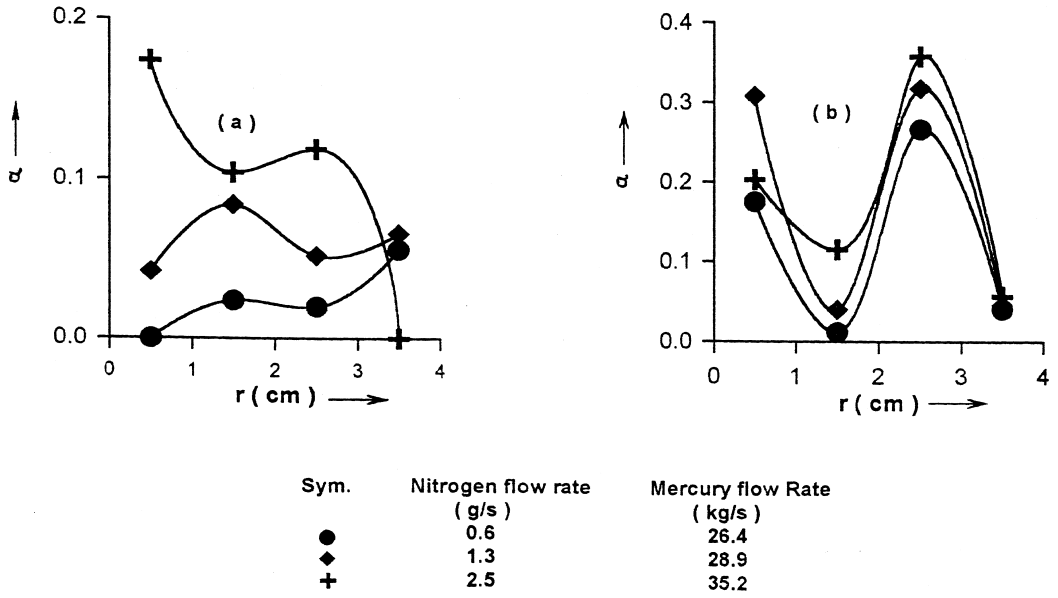

Fig. 5. Measured void fraction profiles for low gas flow rates at two locations in the riser. (a) $Z = 1.1$ m; (b) $Z = 2.8$ m.

in the void profile is not explicitly shown in the figure. Further, the flow does not appear to be fully developed in view of low volumetric gas flow rates (Neal and Bankoff, 1965). However, at flow rates above 4.7 g/s, the void profile exhibits monotonic variation with maximum value at the center. In Fig. 6, void profiles measured at locations 1.1 and 2.8 m have been plotted for various nitrogen flow rates above 4.7 g/s. The bars show variation in the right half and left half void values. Further, it is found that at 2.8 m, the profiles are found to be more symmetric with respect to the right and left side as compared to those at the 1.1 m location. This could be due to the absence of cylindrical symmetry in the mixer distributor and also due to the residual entrance effect at 1.1 m distance. From the profiles of the void fraction, area averaged void fraction is calculated.

The error range in the void values is estimated to be around 15% which is based on the repeatability, difference in left and right side measurements, dynamic fluctuations, error in the liquid metal and gas flow rates etc. The slip values are calculated from the measured void fraction, flow rates of gas and liquid metal and pressure using the following relation obtained from mass conservation equations of the fluids.

$$S = \frac{\dot{m}_g}{\dot{m}_l}\frac{\rho_l}{\rho_g}\left(\frac{1}{\alpha} - 1\right). \tag{15}$$

Predicted void fraction and pressure profiles corresponding the measured fluid flow rates have been plotted in Fig. 7. Cross-sectional effects are shown in the Fig. 7(b). The measured void fraction and slip along with the predicted values without and with cross-sectional variation effects are summarized in Table 4. In general, the void fraction is less when cross-sectional variations are included (the corresponding slip values are larger). The maximum deviation

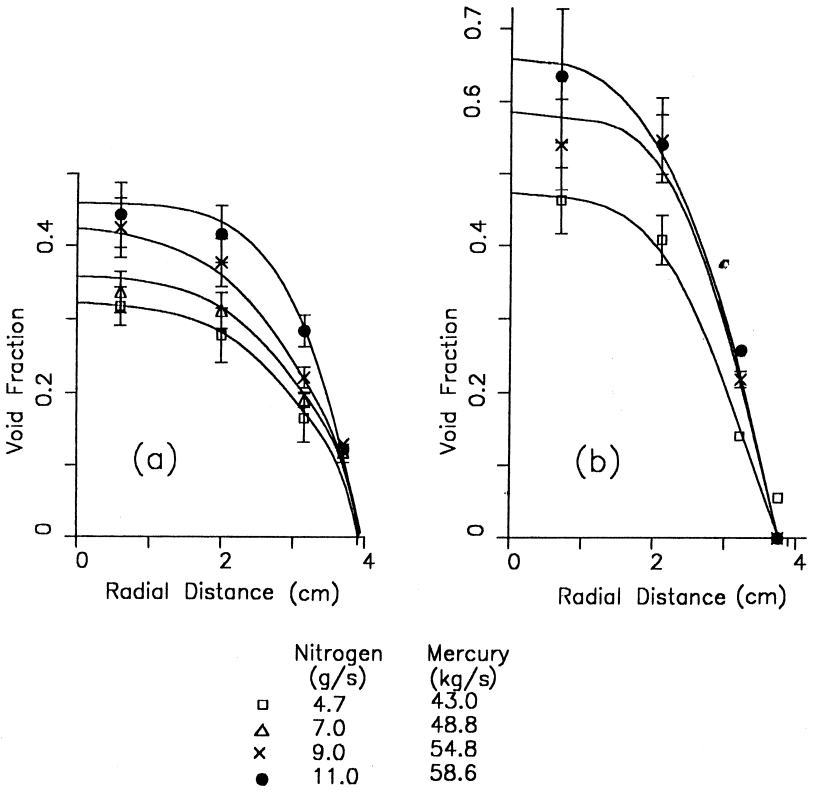

Fig. 6. Measured void fraction profiles for higher gas flow rates at two locations in the riser. (a) $Z = 1.1$ m; (b) $Z = 2.8$ m.

Table 4
Comparison of experimental void fraction and slip with the theoretical models

$\dot{m}_g \times 10^3$ [kg/s]	$\dot{m}_l$ [kg/s]	α	α_{cs}	α [exptl]	S	S_{cs}	S [exptl]
Z = 1.1 m							
2.5	35.3	0.11	0.10	0.15	1.3	1.5	1.2
4.7	43.0	0.18	0.16	0.20	1.2	1.5	1.0
7.0	48.8	0.23	0.20	0.25	1.2	1.4	1.2
9.0	54.8	0.27	0.23	0.29	1.2	1.4	1.1
11.0	58.6	0.30	0.26	0.32	1.1	1.4	1.2
Z = 2.8 m							
0.6	26.4	0.06	0.05	0.03	1.4	1.6	1.8
1.3	28.9	0.10	0.10	0.07	1.3	1.6	1.1
2.5	35.3	0.17	0.15	0.18	1.2	1.5	1.8
4.7	43.0	0.25	0.23	0.26	1.2	1.5	1.3
7.0	48.8	0.31	0.27	0.31	1.2	1.5	1.5
9.0	54.8	0.36	0.31	0.36	1.2	1.5	1.6
11.0	58.6	0.40	0.35	0.40	1.1	1.5	1.4

cs: cross-sectional variations accounted.

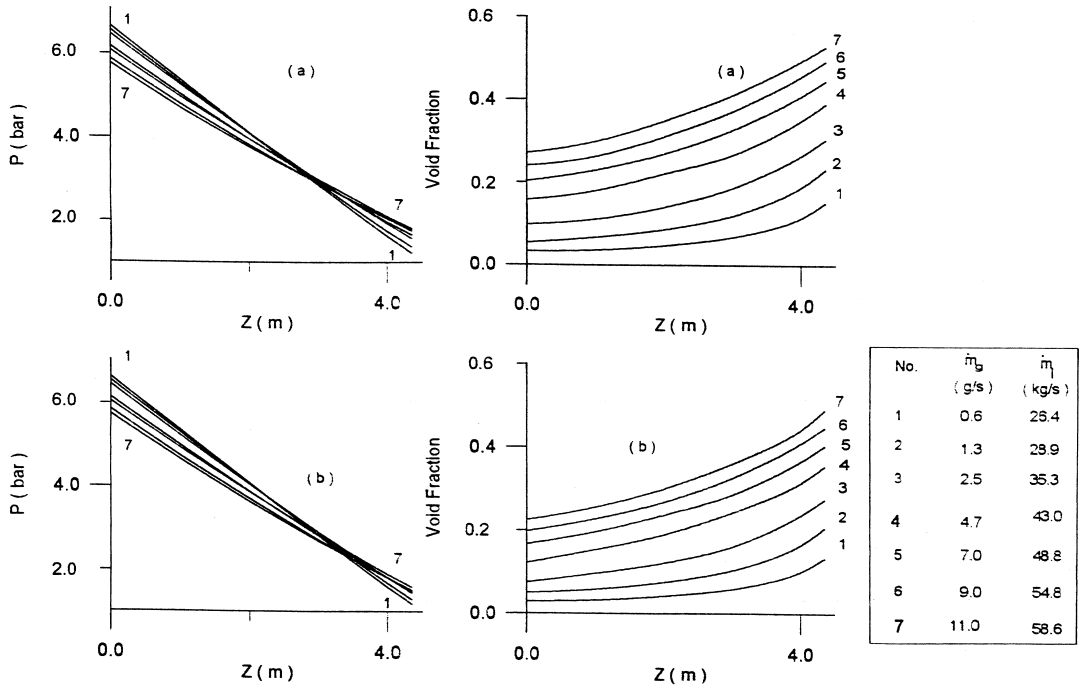

Fig. 7. Predicted pressure and void fraction variation along the riser length. (a) Without cross-sectional effects; (b) with cross-sectional effects.

between the experimental and the theoretical values is less than 10% and is less than 20% when the cross-sectional variations are included. Calculated slip value based on the experimental void fraction for 4.7 g/s are $x = 1.1$ m is around 1.0, which is low and can be attributed to the experimental error in the void fraction measurement. The deviation for the same flow rate between the experimental slip and the predicted value if 20% and is 50% when the cross-sectional effects are included. For the 2.5 g/s flow rate at $x = 2.8$ m, the deviation between the experimental slip and the predicted value if 33% when cross-sectional effects are not included and is 17% with cross sectional effects. For the rest of the flows, the maximum deviation is less than 25% and 27% , respectively, without and with the cross-sectional effects. The measured pressure data are compared with the predicted values in Table 5. As can be seen, for 11.0 g/s flow rate at 3.48 m location, the maximum deviation is 22% and is 13% when cross-sectional effects are included. For the rest of the data, the maximum deviation is less than 13% and when the cross-sectional effects are included, it is less than 8%.

5. Summary and conclusion

A two fluid model consisting of one-dimensional continuity equations for gas–vapor and liquid metal, gas–vapor momentum equation, combined momentum equation along with the auxiliary equations has been developed for vertical two-phase upward high density liquid metal

Table 5
Comparison of predicted and measured pressure values

$\dot{m}_g \times 10^3$ [kg/s]	$\dot{m}_l$ [kg/s]	P [bar]	P_{cs} [bar]	P(exptl) [bar]
Z = 0.64 m				
0.6	26.4	5.84	5.83	5.93
1.3	28.9	5.76	5.76	5.85
2.5	35.3	5.69	5.68	5.74
4.7	43.0	5.43	5.41	5.59
7.0	48.8	5.34	5.33	5.39
9.0	54.8	5.14	5.13	5.22
11.0	58.6	5.03	5.03	4.81
Z = 1.93 m				
0.6	26.4	4.19	4.18	4.29
1.3	28.9	4.17	4.15	4.22
2.5	35.3	4.17	4.13	4.12
4.7	43.0	4.02	3.95	3.97
7.0	48.8	4.01	3.94	3.82
9.0	54.8	3.85	3.78	3.73
11.0	58.6	3.79	3.71	3.43
Z = 2.69 m				
0.6	26.4	3.23	3.21	3.32
1.3	28.9	3.25	3.21	3.24
2.5	35.3	3.31	3.25	3.14
4.7	43.0	3.23	3.13	3.14
7.0	48.8	3.27	3.15	3.04
9.0	54.8	3.14	3.02	2.84
Z = 3.48 m				
0.6	26.4	2.25	2.23	2.34
1.3	28.9	2.32	2.27	2.35
2.5	35.3	2.45	2.36	2.30
4.7	43.0	2.45	2.32	2.25
7.0	48.8	2.53	2.38	2.21
9.0	54.8	2.45	2.27	2.16
11.0	58.6	2.44	2.26	1.87

cs: cross-sectional variations accounted.

flows. The flow regimes consisting of multi-bubble, churn turbulent and slug have been classified based on the Taitel et al. criteria. The interfacial drag force based on Ishii et al. has been used. Bubble diameters at the mixer distributor were calculated using Kumar et al. relations. Two sets of analysis have been carried out, i.e. with and without cross-sectional effects. Experiments were carried out in a nitrogen–mercury system and the void fraction, slip and pressure were determined for the mass fluxes varying from 0.125 to 2.302 kg/sm^2 for nitrogen and 5.52×10^3 to 12.26×10^3 kg/sm^2 for mercury. Over all, measured void fraction matched well with the experimental data within 10% and the slip values within 25%. When the cross sectional effects are included, the maximum deviation is around 20% and 27%

respectively. In general, the measured pressure values deviated by less than 13% and by less than 8% when the cross-sectional effects are included.

Considering the errors in the experimental data, we can conclude that the model which does not include the cross-sectional effects predicts reasonably well the vertical two-phase high density liquid metal flows in the above mass flux ranges. This model can be used for designing the riser of the LMMHD PC systems of gravity type.

Acknowledgements

We are grateful to Mr A. Kakodkar, Director, Bhabha Atomic Research Centre and Mr U. K. Chatterjee, Head, Laser and Plasma Technology Division, for their keen interest and continued support for the development of LMMHD technology. We also gratefully acknowledge Mr D. P. Chakravarthy, Mr M. S. Madanmohan and Mr D. N. Barve for providing the instrumentation support. Part of this study was carried out under the DAE/BRNS Research project no. 36/8/95-R&D-II/671.

References

Barak, A.Z., Blumenau, L., Branover, H., El-Boher, A., Greenspan, E., Spero, E., Sukoriansky, S., 1990. Possibilities for improvement in nuclear reactors using liquid metal magnetohydrodynamic energy conversion. Nuclear Technology 89, 36–51.

Branover, H., 1993. Liquid metal mhd research and development in Israel energy convention and magnetohydrodynamic flows. In: Branover, H., Unger, Y. (Eds.), Progress in Astronautics and Aeronautic. 18. 209–221.

Dounan, J., Zhengie, W., Zhenwan, Yu, Qui, Donming, 1985. Experimental study of void fraction in vertical upward and downward liquid-gas two-phase flow at low velocity, two-phase flow and heat transfer. In: Chen, Xue-jun, Veziriglu, N. (Eds.) Hemisphere, China–US Progress. Publication Corporation, New York, pp. 63–73.

Eckert, S., Gerbeth, G., Thibault, J.P., Mihalache, G., 1993. Some aspect of lmmhd two-phase flows, mhd generator configuration. 7th Beer-Sheva Seminar on MHD flows and Turbulence, Israel , 14–18 Feb.

El-Boher, A., Lesin, S., Unger, Y., Branover, H., 1988. Experimental studies of liquid metal two-phase flows in vertical pipes. In: Shah, R.K., Ganic, E.V., Yang, K. (Eds.) Experimental Heat Transfer, Fluid Mechanics and Thermodynamics. Elsevier Science Publishing Co., pp. 312–319.

Friedel, L., 1979. Improved friction pressure drop correlation for horizontal and vertical two-phase pipe flow. European Two-phase Group Meeting, Ispra E-2, 5–8 June.

Giles, R.V., 1983. Fluid mechanics and hydraulics. Schaum's Outline Series. McGraw-Hill, Singapore.

Idelchik, I.E., 1980. Handbook of Hydraulic Resistance. Hemisphere, New York.

Ishii, M., Mishima, K., 1984. Two-fluid model and hydrodynamic constitutive relations. Nuclear Engineering and Design 82, 107–126.

Ishii, M., Zuber, N., 1979. Drag coefficient and relative velocity in bubble, droplet or particulate flows. A. I. Ch. E. Journal 25, 843–855.

Kumar, A., Degaleesan, T.E., Laddha, G.S., Hoelscher, H.E., 1976. Bubble swarm characteristic in bubble columns. The Canadian Journal of Chemical Engineering 54, 503–508.

Lahey, R.T., Jr, Cheng, L.Y., Drew, D.A., Flaherty, J.E., 1980. The effect of virtual mass on the numerical stability of accelerating two-phase flows. International Journal of Multiphase Flow 6, 281–294.

Mond, M., Sukoriansky, 1984. An analytical model for bubbly flow. 4th Beer-Sheva seminar on MHD flows and Turbulence, Israel, pp. 329–339.

Munshi, P., Vaidya, M.S., 1993. A sensitivity study of Poisson's corruption in tomographic measurements for air–water flows. Trans. American Nuclear Society 68, 234–236.

Neal, L.G., Bankoff, S.G., 1965. Local parameters in cocurrent mercury–nitrogen flow. A. I. Ch. E. Journal 11, 624–635.

Satyamurthy, P., Thiyagarajan, T.K., Venkatramani, N., 1994. Void fraction profile measurement in two-phase liquid metal flows: correction for finite beam size of the gamma-rays. 2nd International Conference on Energy Transfer in Magnetohydrodynamic Flows, France.

Satyamurthy, P., Thiyagarajan, T.K., Venkatramani, N., 1995. Conceptual scheme for electrical power generation from nuclear waste using liquid metal magnetohydrodynamic energy converter. Energy Conversion and Management 36, 975–987.

Serizawa, A., Michiyoshi, I., 1973. Void fraction and pressure drop in liquid metal two-phase flow. Journal of Nuclear Science and Technology 10, 435–445.

Taitel, Y., Bornea, D., Duckler, A.E., 1980. Modeling flow pattern transition for steady upward gas-liquid flow in vertical tubes. A. I. Ch. E. Journal 26, 345–354.

Thiyagarajan, T.K., Dixit, N.S., Satyamurthy, P., Venkatramani, N., Rohatgi, V.K., 1991. Gamma-ray attenuation method for void fraction measurement in fluctuating two-phase liquid metal flows. Measurement Science and Technology 2, 69–74.

Thiyagarajan, T.K., Satyamurthy, P., Dixit, N.S., Venkatramani, N., Garg, A., Kanvinde, N.R., 1995. Void fraction profile measurements in the two-phase mercury–nitrogen flows using gamma-ray attenuation method. Experimental Thermal and Fluid Sciences 10, 347–354.

Unger, Y., El-Boher, A., Lesin, S., Branover, H., 1986. Two-phase liquid metal gas flows in vertical flows in pipes. 9th International Conference on MHD electrical power generation, Japan, pp. 743–752.

Zuber, N., 1964. On the dispersed two-phase flow on the laminar flow regime. Chemical Engineering Science 19, 897–917.